MATERIALS SCIENCE

2D titanium carbide (MXene) for wireless communication

Asia Sarycheva[1], Alessia Polemi[1], Yuqiao Liu[2], Kapil Dandekar[2], Babak Anasori[1]*, Yury Gogotsi[1]*

With the development of the Internet of Things (IoT), the demand for thin and wearable electronic devices is growing quickly. The essential part of the IoT is communication between devices, which requires radio-frequency (RF) antennas. Metals are widely used for antennas; however, their bulkiness limits the fabrication of thin, lightweight, and flexible antennas. Recently, nanomaterials such as graphene, carbon nanotubes, and conductive polymers came into play. However, poor conductivity limits their use. We show RF devices for wireless communication based on metallic two-dimensional (2D) titanium carbide (MXene) prepared by a single-step spray coating. We fabricated a ~100-nm-thick translucent MXene antenna with a reflection coefficient of less than −10 dB. By increasing the antenna thickness to 8 μm, we achieved a reflection coefficient of −65 dB. We also fabricated a 1-μm-thick MXene RF identification device tag reaching a reading distance of 8 m at 860 MHz. Our finding shows that 2D titanium carbide MXene operates below the skin depth of copper or other metals as well as offers an opportunity to produce transparent antennas. Being the most conductive, as well as water-dispersible, among solution-processed 2D materials, MXenes open new avenues for manufacturing various classes of RF and other portable, flexible, and wearable electronic devices.

INTRODUCTION

Fueled by societal demand for devices that enable active, efficient, and integrated lifestyles, there is an ever-increasing need for portable and wearable electronics. With the rising development of the Internet of Things (IoT), those devices need a concealed integration of radio communication electronics (1) without sacrificing lightweight and transportability. Therefore, the development of new routes of antenna fabrication is needed.

Common antennas use metals, such as silver, copper, or aluminum, as conductors. The use of metals is dictated by the need of high electrical conductivity for transmitting and receiving radio waves. However, the performance of thin metal antennas is limited by an intrinsic property called the skin depth, which is the thickness of the material where the electrical current responsible for the radio-frequency (RF) radiation is effectively flowing. In a bulk metal, more than 98% of the electrical current flows within a layer with a thickness of about four times of the skin depth from the surface (2).

The skin depth is frequency-dependent. For example, the skin depth of copper at the Wi-Fi or Bluetooth frequency (2.4 GHz) is 1.33 μm. Silver and aluminum have skin depths of 1.29 and 1.67 μm, respectively, which means that the thickness of these metal antennas should be at least ~5 μm for these applications to ensure a sufficient space for the electrical current to flow. In wearable and transparent devices, skin depth becomes a limiting factor, making thin antenna fabrication challenging. Other approaches, such as metallic yarn manufacturing (3), have been used. However, fabricating flexible, conformal, easy to handle, thin metal antennas is not an easy task.

To overcome these challenges, alternative materials such as conductive polymers or nanomaterials have been explored in the field of RF wireless communication device manufacturing. These materials have to be easily processable, so they can be coated into conductive films. For example, one of the common conductive polymers, poly(3,4-ethylenedioxythiophene) polystyrene sulfonate, was used to produce

an optically transparent dipole antenna (4) having a gain of −4 dB, translating into 40% of transmitted power loss from the antenna. To improve the performance, composites with metal nanoparticles have been used. For example, 150-μm-thick stretchable electrospun fiber mats dip-coated by silver nanoparticles, with an electrical conductivity of ~5400 S/cm, were used to design flexible antennas (5). In the past decade, carbon-based nanomaterials have been extensively investigated in wireless communication applications. For example, carbon onions (6), carbon nanotubes (CNTs) (7, 8), and graphene (9, 10) were used for the fabrication of antennas. Other two-dimensional (2D) materials, such as the metallic 1T phase of MoS_2, were explored for fabrication of electronic devices operating in the gigahertz region (11). Despite promising experimental results of the use of 1D and 2D nanomaterials, the theoretical understanding of these devices remains limited. Specifically, all these nanomaterials perform at thicknesses below their predicted skin depth (see more details in the Supplementary Materials). For example, the conductivity of a graphene antenna was reported (12) to be 43 S/cm, and at an operating frequency of 10 GHz, the skin depth is calculated to be 77 μm. However, the reported graphene antenna was only 7.7 μm thick (12), and the reported gain reached 1.9 dB. This could possibly be explained by different mechanisms of wave propagation in 2D and 1D materials. In particular, the behavior of waves propagating through nanomaterials at the radio frequencies has been investigated (13, 14), but a full theoretical insight has not yet been reached.

Despite the promising performances of carbon nanomaterials and other 2D materials in the RF communication application, their electrical conductivity is still relatively low, and several steps, such as incorporating conductive additives, are required to achieve a reasonable RF performance (6–12). Among all solution-processed 2D materials known to date, the as-deposited 2D titanium carbide MXene films have shown to have high electrical conductivities of up to 5000 to 10,000 S/cm, which exceed those of other solution-processed 2D materials (15) and makes them the best candidate for antenna fabrication. The 2D titanium carbide with a formula of Ti_3C_2 is a member of a family of 2D transition metal carbides and nitrides, known as MXenes, with a formula of $M_{n+1}X_n$, where M is an early transition metal (such as Ti, V, Nb, and Mo) and X is carbon or nitrogen. Chemically

[1]Department of Materials Science and Engineering and A.J. Drexel Nanomaterials Institute, Drexel University, Philadelphia, PA 19104, USA. [2]Department of Electrical and Computer Engineering, Drexel University, Philadelphia, PA 19104, USA.
*Corresponding author. Email: ba323@drexel.edu (B.A.); gogotsi@drexel.edu (Y.G.)

synthesized MXenes using acidic fluoride solutions have surface terminations such as –O, –F, and –OH (*16*). These surface terminations account for hydrophilicity of MXene flakes, which can be delaminated into colloidal solutions of single 2D flakes (*16*). MXene flakes are negatively charged with ξ potential from −30 to −80 mV (*17*), forming stable colloidal solution in various organic and non-organic solvents (*18*). The as-synthesized MXene clay or the colloidal solution can be processed into flexible, conductive thin films without any binder via various methods including rolling (*19*), spraying (*20*), spin coating, drop casting (*21*), and printing, which makes MXene a great candidate for RF applications.

In 2016, a thin film of Ti_3C_2 and its composites have shown electromagnetic interference (EMI) shielding capabilities comparable to metals and outperforming other nanomaterials of similar thicknesses (*22*). Here, we report on the first flexible MXene dipole antennas with thicknesses from 62 nm to 8 μm operating in the Wi-Fi and Bluetooth frequency bands, as well as an ultrahigh-frequency RF identification device (RFID) tag. In addition, by preparing a MXene transmission line (TL), we have studied radio wave propagation through MXene films.

RESULTS AND DISCUSSION

The MXene synthesis procedure can be found in the Supplementary Materials. Briefly, Ti_3C_2 MXene was synthesized from Ti_3AlC_2 by etching its aluminum layers in fluoride-containing acidic solutions (*23*). When selective etching was completed, we washed the MXene powder in deionized (DI) water to raise the acidic pH to neutral. Further delamination occurred due to intercalation of Li^+ ions between the layers and resulted in a stable aqueous colloidal solution of Ti_3C_2 flakes (Fig. 1A) suitable for film fabrication via filtration, spraying, printing, or spin coating. In our study, we focus on producing thin films by spraying technique for film thicknesses below ~1.4 μm and vacuum-assisted filtration for thicknesses above 1 μm (Fig. 1A).

We used an air spray gun to spray MXene aqueous colloidal solution (MXene ink; Fig. 1A). To show the diversity of possible substrates, we sprayed the MXene ink on relatively smooth polyethylene terephthalate (PET) sheets and on rough substrates such as cellulose paper (fig. S1 and table S1; detailed procedure can be found in the Supplementary Materials). To improve adhesion to the surface, we used oxygen plasma treatment on the substrate before the deposition. The commercially available PET substrate that we used had a surface roughness at the nanometer scale (fig. S2). The advantage of spraying on PET is that it provides a uniform coverage with thicknesses of less than 1 μm. For the antenna measurements, we only focus on the spray-coated films on PET with thicknesses ranging from 62 nm to ~1.4 μm (Fig. 1B). The cross-sectional SEM image of the sprayed MXene film on PET shows a stacked structure of MXene layers (Fig. 1C and fig. S3). The top view of the spray-coated film is shown in Fig. 1C (inset), revealing individual Ti_3C_2 flakes (marked with dotted lines) interconnected to each other and forming a continuous conductive film.

To fabricate MXene films with thicknesses larger than ~1 μm, we vacuum-filtered the MXene colloidal solution—the same solution that we used for spray coating. To compare the MXene films made via different fabrication routes (sprayed or filtered), we used XRD (Fig. 1D). Because MXene synthesis involves aqueous solutions, water molecules are present between the individual 2D flakes. To remove the interlayer water and increase MXene film conductivity, we treated them at 150°C for 24 hours under vacuum. The XRD pattern for the as-sprayed

samples on the PET substrate has a broad (002) peak around 5.2°, showing an interlayer spacing of ~17 Å for the MXene film. After thermal treatment, the peak shifts to 6.1° and sharpens, which indicates improved flake alignment and a smaller interlayer spacing of ~14.5 Å. However, the as-filtered films have even smaller interlayer spacing of ~12.9 Å, and thermal treatment further removes the water in between the 2D MXene sheets and leads to an interlayer spacing of ~10.6 Å. Hence, filtered films have less confined water in the structure and higher conductivities, as discussed below.

A common parameter for characterization of materials for RF circuits is sheet resistance. Figure 1E shows the dependence of the sheet resistance on thickness, measured using a linear four-point probe resistance measurement. Conductivity of the filtered freestanding film with a thickness of 8 μm was 8000 S/cm. MXene film thickness measurements are described in the Supplementary Materials. The thicknesses of ~600 nm and less were determined using an ultraviolet-visible (UV-vis) spectrometer from the calibration curve (*20*) available for the spraying method. The procedure is also described in the Supplementary Materials. Sheet resistance of the thickest sprayed film (1.4 μm thick) reached 0.77 ± 0.08 ohms/sq (Fig. 1E). The thinnest sprayed film exhibited 49% of transmittance of light at 550 nm and a sheet resistance of 47 ± 8 ohms/sq. The 49% transmittance corresponds to a thickness of around 62 nm. As shown in Fig. 1E, the sheet resistance increases significantly for thicknesses ≤100 nm, which is probably caused by interrupted flake connections due to the limitations of manual spray coating method.

We have prepared and tested three different kinds of MXene devices to explore three different ways for achieving RF communication and demonstrating relevant MXene properties: (i) a dipole antenna for exploring radiation properties, (ii) a TL for wave propagation properties, and (iii) an RFID tag to study the backscattering.

A Ti_3C_2 straight dipole antenna is easy to manufacture, making it ideal for the first MXene antenna study. Half-wave dipole antennas are commonly used for broadcasting, cellular phones, and wireless communication due to their omnidirectional properties. We designed the MXene dipole at 2.4 GHz, which is widely used for Wi-Fi and Bluetooth applications. The total length of the dipole is about 62 mm (Fig. 2A), which corresponds to half wavelength at a working frequency of 2.4 GHz. To quantify the antenna performance, we studied return loss and the radiation properties of the antenna.

The scattering parameter S_{11} at the input port was recorded using a vector network analyzer (VNA) to quantify the return loss of the antenna, which indicates the amount of power reflected at the port with respect to what is delivered as input (*2*). The amount of power that is not reflected goes into the antenna and is partly radiated as energy or is lost in the material as ohmic losses. The return loss shows the 50-ohm impedance matching condition, as shown in Fig. 2B and fig. S4 for Ti_3C_2 MXene antennas with thicknesses from 62 nm to 8 μm. MXene antennas show good impedance matching. Figure 2B shows Ti_3C_2 antennas with thicknesses from 114 nm to 8 μm, and the peak return loss results from −12 to −65 dB, respectively. Peak return losses lower than −10 dB are commonly considered satisfactory impedance matching. MXene return loss is increasing with decreasing of the antenna thickness (table S2). This trend could partially correspond to the decrease of conductivity, but mostly, it is related to the change of resistance with length, which decreases more markedly in the thinner films because of manual spraying, as shown in Fig. 1E.

For the 8-μm-thick MXene antenna, we measured a reflection coefficient of approximately −65 dB, which, to our knowledge, outperforms
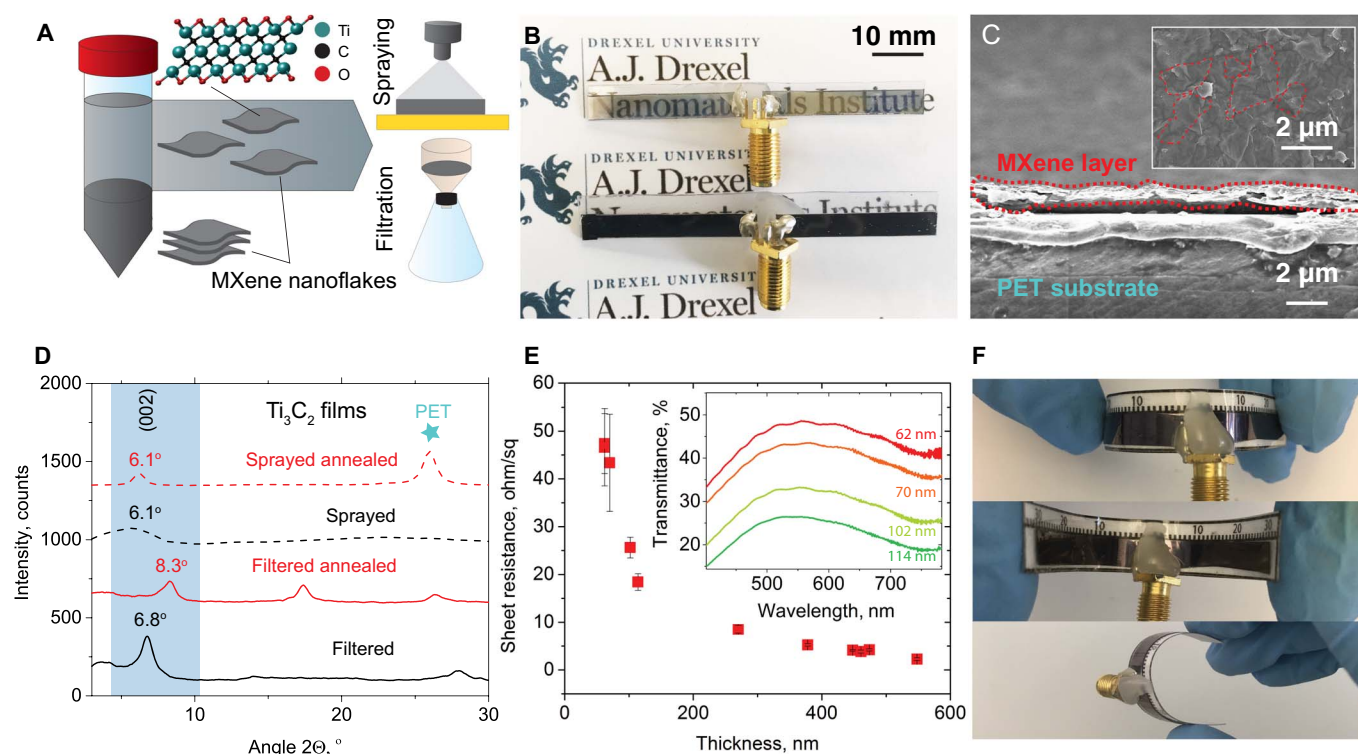
Fig. 1. Ti$_3$C$_2$ MXene films and antennas and their processing. (**A**) Schematic of multilayered and delaminated forms of 2D Ti$_3$C$_2$ MXene. Top: Atomistic model of a single Ti$_3$C$_2$T$_x$ flake. A single Ti$_3$C$_2$T$_x$ flake has a thickness of ~1 nm. Delaminated single flakes form a stable colloidal solution (MXene ink) and can be processed into freestanding films by vacuum-assisted filtration or sprayed with an air spray gun onto a substrate. (**B**) Digital photo showing 62-nm-thick (top) and 1.4-μm-thick (bottom) MXene dipole antennas. (**C**) Cross-sectional scanning electron microscopy (SEM) image of the sprayed MXene (red dashed line). The inset is a top view of the film, where individual Ti$_3$C$_2$ flakes are highlighted with red dotted lines. (**D**) X-ray diffraction (XRD) patterns of MXene films prepared by vacuum-assisted filtration (black solid line) and after treatment in vacuum at 150°C (red solid line). Thermal treatment of the MXene film shifts the (002) MXene peak position from 6.8° to 8.3°. The same comparison was made with the sprayed 1.4-μm-thick MXene film on PET, as-sprayed MXene film (black dashed line), and the film was heated in vacuum at 150°C (red dashed line). Annealing changed the (002) peak position from ~5° to 6.1° and increased its intensity. The peak around 23° is attributed to the PET substrate. (**E**) Sheet resistance versus thickness of sprayed MXene films. Inset shows transmittance in the visible range of light for the thinnest antennas. (**F**) Digital photos of sprayed MXene dipole antennas bent at different curvatures, showing the stability of the deposited layer and its adhesion to the substrate.

all the nanomaterial antennas of comparable thickness measured to date, including silver inks and paste. Even with a 1.4-μm-thick MXene antenna made by spraying MXene water-based colloidal solution, we were able to obtain a reflection coefficient of approximately −36 dB, outperforming the 7-μm-thick printed graphene (*12*), laminated graphene (*10*), or printed silver ink (*24*) (table S2). Figure S5 summarizes the results presented in table S2 and shows that Ti$_3$C$_2$ MXene dipole antennas exhibit the highest performance-to-thickness ratio. The increase in return loss at very low thicknesses (that is, smaller than 100 nm) could be explained by the lack of film uniformity due to the PET substrate roughness and the manual spray deposition method. In addition, we fabricated dipole antennas with different MXene materials, Ti$_2$C and Mo$_2$TiC$_2$ with ~1-μm-thick filtered films. Both Ti$_2$C and Mo$_2$TiC$_2$ had reflection coefficients lower than −10 dB, showing the possibility of making antennas using different kinds of MXenes (fig. S6A). While they did not perform as good as Ti$_3$C$_2$ MXene antennas, the search for the best MXene for antenna applications should continue.

We also performed electrodynamic simulations (CST Microwave Studio), and a good match throughout all the thicknesses was observed (Fig. 2B). CST Microwave Studio is a tool for 3D EM simulations of high-frequency components, which solves Maxwell equations by resorting to specific meshing schemes, both in the time domain and in the

frequency domain (*25*). The dipole antennas are simulated through a thin surface impedance layer with resistivity given by the sheet resistance. We considered a 100-μm-thick layer of lossy substrate as the PET sheet. A discrete 50-ohm port is used as a source.

To quantify the impedance matching at the operating frequency and different thicknesses, the VSWR was calculated (Fig. 2C) using the formula

$$\text{VSWR} = \frac{1 + |S_{11}|}{1 - |S_{11}|}$$

VSWR is the ratio between the peak amplitude and the minimum amplitude of the standing wave that arises from any mismatching condition at the antenna input, which causes input power to be reflected back. A VSWR equal to 1 means that there is no standing wave (S_{11} = −infinity) and that the antenna is ideally matched (*3, 26*). As shown in Fig. 2C, the VSWR is less than 2 for MXene antennas with various thicknesses despite the fact that the surface resistance increases significantly with thicknesses below 100 nm. As a reference, a VSWR equal to 2 means that 11% of the power is reflected.

We also fabricated dipole antennas using commercially available metal foils (aluminum and copper) with different thicknesses (at the
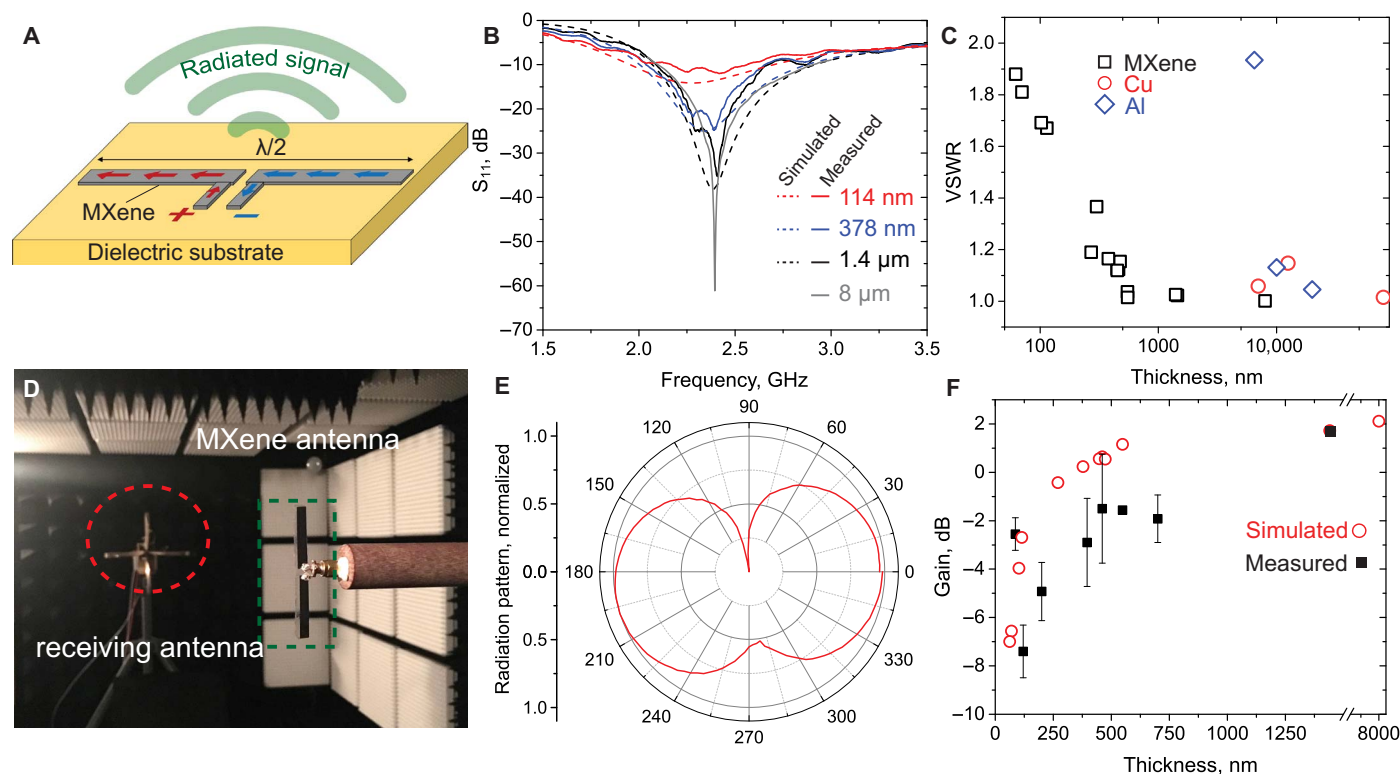
Fig. 2. Ti$_3$C$_2$ MXene antennas and their performance measurements. (**A**) Schematic explaining the working principle of the dipole antenna. The length of the dipole antenna matches half of the wavelength of the radiated signal. (**B**) S$_{11}$ parameter (reflection coefficient) of dipole antennas of various thicknesses (from 114 nm to 8 μm). Measured values are presented as solid lines, and simulated values are presented as dashed lines. (**C**) Voltage standing wave ratio (VSWR) of measured MXene antennas, which represents how efficiently power is transmitted to the antenna and impedance matching. Red and blue symbols represent VSWR of copper and aluminum foils, respectively. (**D**) Digital photo of an experiment in anechoic chamber to measure the radiation pattern of dipole antennas. The Vivaldi antenna was used as the receiving antenna, whereas the radiating antenna was made of MXene. (**E**) Typical radiation pattern of the 8-μm-thick MXene antenna measured in the anechoic chamber. (**F**) MXene antennas' maximum gain versus the antenna thickness. Red circles represent the simulated gain values.

micrometers level) and compared their performance with Ti$_3$C$_2$ MXene antennas (Fig. 2C and fig. S6). Both copper and aluminum antennas showed similar VSWRs at significantly higher thicknesses (Fig. 2C). This shows that Ti$_3$C$_2$ MXene is able to match the impedance at very low antenna thicknesses, which can be easily fabricated by one-step spray coating. However, the antenna might not radiate all the power it receives. Part of this power is lost by ohmic losses, and these will affect the overall efficiency of the antenna. Thus, radiation measurements in the anechoic chamber are required.

We tested MXene dipole antennas in the anechoic chamber, as shown in Fig. 2D. The anechoic chamber is a shielded room that minimizes reflections from the floors, walls, and ceiling to create a "quiet zone" around the antenna under test. The radiation pattern was recorded at an operating frequency of 2.4 GHz by varying the elevation angles. Figure 2E shows the radiation pattern of an 8-μm-thick dipole antenna with typical dipole radiative behavior, where the maximum radiation occurs in the perpendicular direction and nulls are in the longitudinal direction. All radiation patterns can be found in figs. S6B and S7.

To quantify the amount of power effectively radiated from the MXene dipole antenna, the realized gain was calculated with the reference to a standard commercial copper dipole antenna (TDK DP 2400). The gain comparison technique was used (27). The 1.4-μm-thick MXene antenna showed a gain of 1.7 dB. The gain values of all the

MXene antennas presented in Fig. 2F decrease when thickness is reduced. We performed electrodynamic simulations for the MXene antenna gains for the similar thicknesses showing a good match with the data set (Fig. 2F). Simulation shows also that, at a thickness of 8 μm, the MXene antenna exhibits a maximum gain of 2.11 dB, which is converging to the maximum gain of an ideal half-wavelength dipole antenna (2.15 dB). Despite the fact that the predicted skin depth for MXene at a frequency of 2.4 GHz would be 10 μm, Ti$_3$C$_2$ MXene antennas were able to radiate effectively and provide very good matching to the reference impedance at thicknesses below 1 μm.

So far, we have shown MXene antenna performance. In addition, to quantify the losses in a conductive material itself, we investigated the electromagnetic wave propagation in a MXene TL. TLs are basic blocks for a variety of RF devices, such as impedance matching networks, resonators, and filters (2), and are designed to carry the RF signal from one point to another with a minimum loss of energy due to the material losses. TLs also serve as a feeding line for antennas in a circuit. There are various types of TLs. We have selected a coplanar waveguide (CPW) as shown in Fig. 3A, in which the signal is carried by a central conductor, and the two side conductors work as grounding. In our TLs, the central conductor is 1.7 mm wide, and it is spaced 0.5 mm apart from the grounding conductor lines. The total length of the line is 50 mm (Fig. 3A). To characterize a TL, two-port measurements with VNA are required. The recorded parameters were reflection (S$_{11}$) and transmission
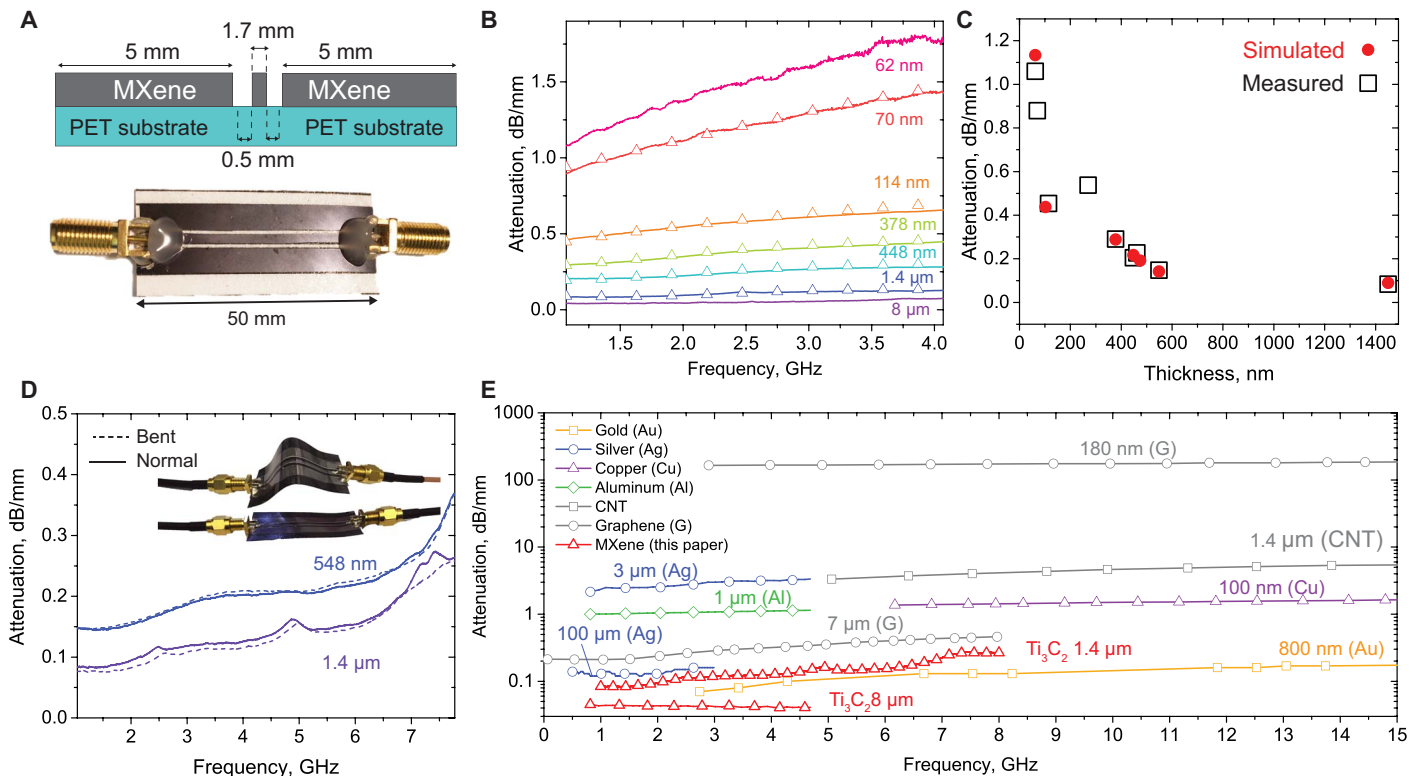
Fig. 3. MXene TLs and their attenuations. (**A**) Schematic and digital photo of the MXene CPW TLs, where MXene was sprayed as a 1.4-μm-thick film. (**B**) Attenuation of MXene films of various thicknesses (from 62 nm to 8 μm) versus frequency measured using MXene TLs. (**C**) Attenuation in dB/mm value at 1 GHz versus sheet resistance for various MXene film thicknesses. (**D**) Attenuation versus frequency of normal (solid line) and bent (dashed line) TLs for MXene film thicknesses of 1.4 μm and 550 nm. No changes could be observed, which shows flexibility of MXene TLs. (**E**) Comparison of attenuation in CPW of different materials: graphene (12, 29), CNT (30), Ag ink (24), Ag-polydimethylsiloxane (31), Au ink (32), Al (33), and Cu (33) with 1.4- and 8-μm-thick Ti_3C_2 MXene films.

(S_{21}) coefficients. The common parameter for estimating the losses in the TL is the attenuation, which can be defined as (12)

$$\text{Attenuation} = \frac{1 - |S_{11}|^2}{|S_{21}|^2}$$

where S_{11} and S_{21} represent the reflection and transmission coefficients, respectively. The attenuation rate can be generalized by normalizing it with respect to the total length. In this way, it becomes a figure of merit that is independent of the actual sample length, and it characterizes material performance in the microwave region.

We fabricated Ti_3C_2 MXene TLs with the same MXene films as we used for the dipole antennas, from film thicknesses of 62 nm to 8 μm. Figure 3B shows attenuation increases with the decrease of the TL film thicknesses. For the TLs of various thicknesses, simulations were carried out, showing a good match with the experimental results. In Fig. 3C, the attenuations at 1 GHz versus sheet resistance are shown together with the simulated data. Reflection (S_{11}), transmission (S_{21}), and attenuation of all the sprayed Ti_3C_2 MXene TLs as well as Al and Cu TLs can be found in fig. S8. To check the flexibility of the MXene TLs, we performed the measurements in bending and normal mode (Fig. 3D). No changes were observed, which makes MXene a great candidate for flexible and wearable wireless communication devices. However, it was previously shown that, with increasing bending cycles, the sheet resistance is increasing by 14% (20). This could possibly be improved by using the spin-coating method with more uniformly distributed flakes.

To compare MXene antennas with other nanomaterials, we plotted the attenuations of different antenna materials from the literature in Fig. 3E. These results show that a 1.4-μm-thick Ti_3C_2 MXene film has about 50 times less losses at 1 GHz than a 7.7-μm-thick graphene–printed film (12) and 300 times less than a silver ink–printed antenna (24), which makes Ti_3C_2 MXene a great candidate for manufacturing ultrathin RF devices.

We also designed and fabricated MXene RFID tags. The geometry and working principal mechanism of RFID antenna is shown in Fig. 4A. Generally, these antennas consist of a radiating part and an impedance matching segment. The matching segment is typically a loop because it serves to match the input impedance of the RFID chip, which is highly capacitive. The matching condition is achieved by enforcing maximum power transfer to ensure both maximum power to the chip and maximum backscattering. In this case, we have used NXP UCODE 7 (see details in fig. S9). In Fig. 4B, the downlink reading distances of three different Ti_3C_2 MXene RFIDs are shown, where each antenna has slightly different loop sizes (fig. S9), thus enabling matching conditions at different frequencies. All the MXene RFID tags exhibit a reading range above 6 m at peak (Fig. 4B), reaching almost 8 m when maximum matching is achieved.

Using MXene for antenna applications, one should know that few-atom-thick single flakes of Ti_3C_2 MXene (~1 nm thick) are stable in inert atmosphere (Ar) but slowly degrade in air due to oxidation. Lipatov et al. (28) showed that, although Ti_3C_2 single-layer flake's conductivity decays in air, Ti_3C_2 remains highly conductive even after exposure to air for 70 hours. Stacks of single-layer Ti_3C_2 flakes, such as filtered or sprayed MXene films, are stable in air. It was shown (15) that a filtered
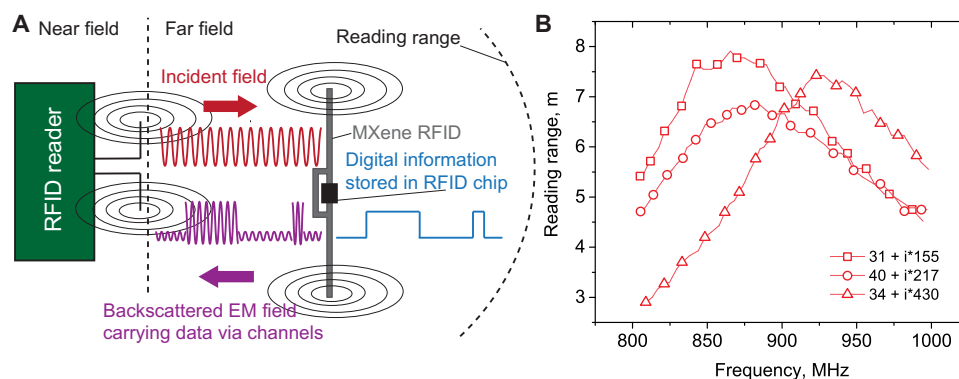
Fig. 4. MXene RFID antennas. (A) General mechanism of RFID working principle. A signal is sent from an RFID reader, received by an RFID antenna connected to an RFID chip. Using the chip, the signal is transformed and backscattered to the reader. **(B)** MXene RFID antenna (1 μm thick) performance with various characteristic impedances. The impedance can be tuned by tuning the design, particularly the loop. The reading range reaches 8 m when matching the impedance of the chip.

film of Ti_3C_2 is stable in air upon storage for 30 days, which can be explained by its compact stacked morphology that protects the inner nanosheets from interacting with humid air. To completely eliminate MXene oxidation, it is possible to laminate final devises or incorporate them inside the protective polymer matrices.

Here, we reported the first RF MXene devices for wireless communication. An 8-μm-thick antenna made from a filmstrip of 2D titanium carbide MXene has a reflection coefficient of −65 dB at 2.4 GHz. We showed the possibility of MXene antenna fabrication by a one-step spray processing from MXene water-based colloidal solution (ink). A 1.4-μm-thick MXene antenna made by spraying showed a gain of up to 1.7 dB. Even at a significantly lower antenna thickness of 62 nm, where we achieve transparency, the antenna is still able to perform, reaching a gain of −7 dB. The decrease in performance could be possibly explained by the limitation of the spray coating and has yet to be optimized. MXene antennas were able to achieve impedance matching in the wide range of thicknesses from 62 nm to 8 μm. Losses caused by the material were determined by assembling a MXene CPW TL. Attenuation of a 1.4-μm-thick MXene film was 50 times lower than that of a 7.7-μm-thick graphene and 300 times less than that of a silver ink–printed antenna. Our results show that MXene antennas work at thicknesses lower than those of the best-known metals and other materials and its predicted skin depth, enabling ultrathin and transparent wireless devices.

MATERIALS AND METHODS
MXene synthesis
The material used in this study was synthesized by selective etching of Al atomic layers from Ti_3AlC_2. One gram of Ti_3AlC_2 powder (particle size, <44 μm; Carbon-Ukraine) was gradually added to a 10 mL solution of 6 ml of 12 M hydrochloric acid, 3 ml of 49% hydrofluoric acid (Sigma-Aldrich), and 1 ml of deionized water (23). The mixture was kept in an ice bath for 10 min and then stirred for 24 hours at room temperature. After etching, the mixture was washed five times by centrifugation in two 150-ml plastic centrifuge tubes at 3500 rpm for 2 min until the pH of the supernatant reached 7 to 6. After that, the sediment was added to a cold 20% solution of lithium chloride (LiCl) in water. The mixture was dispersed by manual shaking, stirred in an ice bath for 10 min, and then stirred at room temperature for 4 hours. After that, MXene was washed three times until the supernatant becomes dark, which is an indication of the beginning of delamination. The unreacted Ti_3AlC_2 and large multilayered Ti_3C_2 particles were separated by centrifugation at

3500 rpm for 1 min, and the collected supernatant was used for spraying. Ti_2C and Mo_2TiC_2 films were made as described elsewhere (22).

Ti_3C_2 spraying on PET
A smooth PET sheet (TruLam, thickness 4 mil, 100 μm) was used as a substrate for spraying due to their transparency and flexibility. Before deposition, PET substrates were cleaned by sonication in 5% Hellmanex III (Sigma-Aldrich) detergent solution for 3 min, followed by sonication in DI water and 190-proof ethanol. Sonication in all cases was limited to 3 min. After drying with compressed air, substrates were cleaned with oxygen plasma to remove residual contamination and make the surface more hydrophilic. Plasma cleaning (Tergeo Plus Plasma Cleaner, PIE Scientific) was done with 4 sccm (standard cubic centimeters per minute) O_2 gas flow, 50 W for 5 min. The chamber was purged with Ar gas after. PET surface was not ideally smooth, as can be seen from the atomic force microscopy (AFM) image in fig. S1. The roughness of cleaned PET reached 23 nm, which could be an obstacle for deposition of very thin MXene films. Ti_3C_2 dispersion in water was loaded into a spray gun. Constant flow of air from a hot gun above the PET substrate provided sufficiently fast drying, making the process easy, fast, and straightforward.

Measuring sheet resistance
Sheet resistance was measured by four-point probe measurements (Jandel ResTest). Each value was measured at least 10 times, and the average value was presented. SD was calculated as an error.

Determining thickness
Because of the limitations of conventional methods of measuring the thickness of thin films, an indirect method based on Beer's law was used. It was shown (20) that the relationship between MXene sprayed film absorption and thickness is linear. Having the relationship between thickness and absorption, one can calculate the thickness. We have measured UV-vis absorption spectra of our films (fig. S3). A blank PET sheet was used as a reference. For thicknesses of the sprayed opaque films, the thickness was calculated by measuring the sheet resistance of the sprayed films and comparing it to the sheet resistance of the freestanding film of known thickness.

Scanning electron microscopy
The SEM was performed with a Zeiss Supra 50VP instrument at an acceleration voltage of 5 kV in InLens mode.

Atomic force microscopy

Bruker MultiMode 8 with a Si tip (Budget Sensors Tap300Al-G; $f_0 = 300$ kHz, $k = 40$ N/m) was used in a standard tapping mode in air.

UV-vis spectroscopy

A UV-vis spectrophotometer (Thermo Scientific Evolution 201) was used. A MXene film sprayed on the PET substrate was placed in a slide holder. A clean PET sheet was used as a reference for the measurements. Spectra were collected in both modes—transmittance and absorbance. To calculate MXene film thickness, the absorbance value at 550 nm was used (20).

X-ray diffraction

Rigaku XRD Smartlab was used to collect XRD patterns. The x-ray wavelength used was 1.5406 Å (Cu Kα) at 40 kV and 44 mA, with a step scan of 0.02°, a 2θ range of 3° to 70°, and a step time of 0.5 s, 10 mm × 10 mm window slit.

Electrodynamic simulations

Electrodynamic simulations were carried out using the commercial software CST Microwave Studio. The software solves Maxwell equations by resorting to the finite integration technique (FIT) in time domain and to a finite element method (FEM) in the frequency domain.

SUPPLEMENTARY MATERIALS

Supplementary material for this article is available at http://advances.sciencemag.org/cgi/content/full/4/9/eaau0920/DC1

Ti$_3$C$_2$ spraying on paper substrates
Skin depth
Fig. S1. Photo of thick MXene film sprayed on PET, label paper, and printing paper.
Fig. S2. AFM image of PET.
Fig. S3. SEM image of a MXene Ti$_3$C$_2$ antenna cross section.
Fig. S4. Reflection coefficient of Ti$_3$C$_2$ MXene.
Fig. S5. Comparison of the return loss of MXene dipole antenna with metals, carbon nanomaterials, conductive polymers, and transparent conductive oxides.
Fig. S6. Characteristics of dipole antennas made of Mo$_2$TiC$_2$, Ti$_2$C MXenes, and metal foils.
Fig. S7. Normalized radiation pattern of Ti$_3$C$_2$ MXene sprayed film antennas.
Fig. S8. Characteristics of transmission lines made of MXene Ti$_3$C$_2$ and metal foils.
Fig. S9. Dimensions of RFID antennas made of Ti$_3$C$_2$ MXene.
Table S1. Sheet resistance of Ti$_3$C$_2$ MXene sprayed on paper.
Table S2. Comparison of the return loss of MXene dipole antennas with other materials.
References (34–44)

REFERENCES AND NOTES

1. A. Al-Fuqaha, M. Guizani, M. Mohammadi, M. Aledhari, M. Ayyash, Internet of things: A survey on enabling technologies, protocols, and applications. *IEEE Commun. Surv. Tutorials* **17**, 2347–2376 (2015).
2. D. M. Pozar, *Microwave Engineering* (John Wiley & Sons, 2009).
3. W. Zeng, L. Shu, Q. Li, S. Chen, F. Wang, X. M. Tao, Fiber-based wearable electronics: A review of materials, fabrication, devices, and applications. *Adv. Mater.* **26**, 5310–5336 (2014).
4. N. J. Kirsch, N. A. Vacirca, E. E. Plowman, T. P. Kurzweg, A. K. Fontecchio, K. R. Dandekar, Optically transparent conductive polymer RFID meandering dipole antenna, in *2009 IEEE International Conference on RFID*, Orlando, FL, 27 to 28 April 2009 (IEEE, 2009), pp. 278–282.
5. M Park, J. Im, M. Shin, Y. Min, J. Park, H. Cho, S. Park, M.-B Shim, S. Jeon, D.-Y. Chang, J. Bae, J. Park, U. Jeong, K. Kim, Highly stretchable electric circuits from a composite material of silver nanoparticles and elastomeric fibres. *Nat. Nanotechnol.* **7**, 803–809 (2012).
6. N. A. Vacirca, J. K. McDonough, K. Jost, Y. Gogotsi, T. P. Kurzweg, Onion-like carbon and carbon nanotube film antennas. *Appl. Phys. Lett.* **103**, 073301 (2013).
7. C. Rutherglen, D. Jain, P. Burke, Nanotube electronics for radiofrequency applications. *Nat. Nanotechnol.* **4**, 811–819 (2009).
8. I. Puchades, J. E. Rossi, C. D. Cress, E. Naglich, B. J. Landi, Carbon nanotube thin-film antennas. *ACS Appl. Mater. Interfaces* **8**, 20986–20992 (2016).
9. K. Y. Shin, J. Y. Hong, J. Jang, Micropatterning of graphene sheets by inkjet printing and its wideband dipole-antenna application. *Adv. Mater.* **23**, 2113–2118 (2011).
10. X. Huang, T. Leng, X. Zhang, J. C. Chen, K. H. Chang, A. K. Geim, K. S. Novoselov, Z. Hu, Binder-free highly conductive graphene laminate for low cost printed radio frequency applications. *Appl. Phys. Lett.* **106**, 203105 (2015).
11. H.-Y. Chang, M. N. Yogeesh, R. Ghosh, A. Rai, A. Sanne, S. Yang, N. Lu, S. K. Banerjee, D. Akinwande, Large-area monolayer MoS$_2$ for flexible low-power RF nanoelectronics in the GHz regime. *Adv. Mater.* **28**, 1818–1823 (2016).
12. X. Huang, T. Leng, K. H. Chang, J. C. Chen, K. S. Novoselov, Z. Hu, Graphene radio frequency and microwave passive components for low cost wearable electronics. *2D Mater.* **3**, 025021 (2016).
13. P. J. Burke, L. Shengdong, Y. Zhen, Quantitative theory of nanowire and nanotube antenna performance. *IEEE Trans Nanotechnol.* **5**, 314–334 (2006).
14. G. Deligeorgis, M. Dragoman, D. Neculoiu, D. Dragoman, G. Konstantinidis, A. Cismaru, R. Plana, Microwave propagation in graphene. *Appl. Phys. Lett.* **95**, 073107 (2009).
15. C. J. Zhang, B. Anasori, A. Seral-Ascaso, S. H. Park, N. McEvoy, A. Shmeliov, G. S. Duesberg, J. N. Coleman, Y. Gogotsi, V. Nicolosi, Transparent, flexible, and conductive 2D titanium carbide (MXene) films with high volumetric capacitance. *Adv. Mater.* **29**, 1702678 (2017).
16. B. Anasori, M. R. Lukatskaya, Y. Gogotsi, 2D metal carbides and nitrides (MXenes) for energy storage. *Nat. Rev. Mater.* **2**, 16098 (2017).
17. Y. Ying, Y. Liu, X. Wang, Y. Mao, W. Cao, P. Hu, X. Peng, Two-dimensional titanium carbide for efficiently reductive removal of highly toxic chromium(VI) from water. *ACS Appl. Mater. Interfaces* **7**, 1795–1803 (2015).
18. K. Maleski, V. N. Mochalin, Y. Gogotsi, Dispersions of two-dimensional titanium carbide MXene in organic solvents. *Chem. Mater.* **29**, 1632–1640 (2017).
19. M. Ghidiu, M. R. Lukatskaya, M.-Q. Zhao, Y. Gogotsi, M. W. Barsoum, Conductive two-dimensional titanium carbide 'clay' with high volumetric capacitance. *Nature* **516**, 78–81 (2014).
20. K. Hantanasirisakul, M.-Q. Zhao, P. Urbankowski, J. Halim, B. Anasori, S. Kota, Y. Gogotsi, Fabrication of Ti$_3$C$_2$T$_x$ MXene transparent thin films with tunable optoelectronic properties. *Adv. Electronic Mater.* **2**, 1600050 (2016).
21. A. D. Dillon, M. J. Ghidiu, A. L. Krick, J. Griggs, S. J. May, Y. Gogotsi, M.W. Barsoum, A.T. Fafarman, Highly conductive optical quality solution-processed films of 2D titanium carbide. *Adv. Funct. Mater.* **26**, 4162–4168 (2016).
22. F. Shahzad, M. Alhabeb, C. B. Hatter, B. Anasori, S. M. Hong, C. M. Koo, Y. Gogotsi, Electromagnetic interference shielding with 2D transition metal carbides (MXenes). *Science* **353**, 1137–1140 (2016).
23. M. Alhabeb, K. Maleski, B. Anasori, P. Lelyukh, L. Clark, S. Sin, Y. Gogotsi, Guidelines for synthesis and processing of two-dimensional titanium carbide (Ti$_3$C$_2$T$_x$ MXene). *Chem. Mater.* **29**, 7633–7644 (2017).
24. A. Chiolerio, M. Cotto, P. Pandolfi, P. Martino, V. Camarchia, M. Pirola, G. Ghione, Ag nanoparticle-based inkjet-printed planar transmission lines for RF and microwave applications: Considerations on ink composition, nanoparticle size distribution and sintering time. *Microelectron. Eng.* **97**, 8–15 (2012).
25. M. Clemens, T. Weiland, Discrete electromagnetism with the finite integration technique. *Prog. Electromagn. Res.* **32**, 65–87 (2001).
26. C. A. Balanis, *Antenna Theory: Analysis and Design, 3rd Edition* (John Wiley & Sons, 2005).
27. A. O. Michael, On the antenna gain formula. *Int. J. Appl. Sci. Technol.* **3**, 43–49 (2013).
28. A. Lipatov, M. Alhabeb, M. R. Lukatskaya, A. Boson, Y. Gogotsi, A. Sinitskii, Effect of synthesis on quality, electronic properties and environmental stability of individual monolayer Ti$_3$C$_2$ MXene flakes. *Adv. Electron. Mater.* **2**, 1600255 (2016).
29. Z. Wang, X. Shu, P. Peng, Y. Jia, L. Ren, X. Gong, X. Zhang, R. Huang, J. Wen, Y. Fu, Low insertion loss of 200 µm-long graphite coplanar waveguide. *Appl. Phys. Lett.* **108**, 033104 (2016).
30. M. Dragoman, K. Grenier, D. Dubuc, L. Bary, E. Fourn, R. Plana, E. Flahaut, Experimental determination of microwave attenuation and electrical permittivity of double-walled carbon nanotubes. *Appl. Phys. Lett.* **88**, 153108 (2006).
31. Z. Chen, J. Xi, W. Huang, M. M. F. Yuen, Stretchable conductive elastomer for wireless wearable communication applications. *Sci. Rep.* **7**, 10958 (2017).
32. H. S. Gamble, B. M. Armstrong, S. J. N. Mitchell, Y. Wu, V. F. Fusco, J. A. C. Stewart, Low-loss CPW lines on surface stabilized high-resistivity silicon. *IEEE Microwave Wireless Compon. Lett.* **9**, 395–397 (1999).
33. P. Sarafis, C.-L. Hsu, P. Benech, A. G. Nassiopoulou, Cu nanolines for RF interconnects: Electrical characterization. *IEEE Trans. Electron. Devices* **62**, 1537–1543 (2015).
34. H. Koga, T. Inui, I. Miyamoto, T. Sekiguchi, M. Nogi, K. Suganuma, A high-sensitivity printed antenna prepared by rapid low-temperature sintering of silver ink. *RSC Adv.* **6**, 84363–84368 (2016).
35. D.-Y. Shin, Y. Lee, C. H. Kim, Performance characterization of screen printed radio frequency identification antennas with silver nanopaste. *Thin Solid Films* **517**, 6112–6118 (2009).
36. A. Chauraya, W. G. Whittow, J. Y. C. Vardaxoglou, Y. Li, R. Torah, K. Yang, J. Tudor, Inkjet printed dipole antennas on textiles for wearable communications. *IET Microwave Antennas Propag.* **7**, 760–767 (2013).

37. Y. Bayram, Y. Zhou, B. S. Shim, S. Xu, J. Zhu, N. A. Kotov, J. L. Volakis, E-textile conductors and polymer composites for conformal lightweight antennas. *IEEE Trans. Antennas. Propag.* **58**, 2732–2736 (2010).

38. Q.-Y. Tang, Y.-M. Pan, Y. C. Chan, K. W. Leung, Frequency-tunable soft composite antennas for wireless sensing. *Sens. Actuators A Phys.* **179**, 137–145 (2012).

39. T. A. Elwi, H. M. Al-Rizzo, D. G. Rucker, E. Dervishi, Z. Li, A. S. Biris, Multi-walled carbon nanotube-based RF antennas. *Nanotechnology* **21**, 045301 (2010).

40. N. Guan, H. Furuya, D. Delaune, K. Ito, Radiation efficiency of monopole antenna made of a transparent conductive film, in *2007 IEEE Antennas and Propagation Society International Symposium*, Honolulu, HI, 9 to 15 June 2007 (IEEE, 2007), pp. 221–224.

41. J. S. Lee, M. Kim, C. Lee, S. Cho, J. Oh, J. Jang, Platinum-decorated reduced graphene oxide/polyaniline:poly(4-styrenesulfonate) hybrid paste for flexible dipole tag-antenna applications. *Nanoscale* **7**, 3668–3674 (2015).

42. K.-Y. Shin, M. Kim, J. S. Lee, J. Jang, Highly omnidirectional and frequency controllable carbon/polyaniline-based 2D and 3D monopole antenna. *Sci. Rep.* **5**, 13615 (2015).

43. S. Z. Sajal, B. D. Braaten, V. R. Marinov, A microstrip patch antenna manufactured with flexible graphene-based conducting material, in *2015 IEEE International Symposium on Antennas and Propagation & USNC/URSI National Radio Science Meeting*, Vancouver, British Columbia, Canada, 17 to 25 July 2015 (IEEE, 2015), pp. 2415–2416.

44. A. Lamminen, K. Arapov, G. De With, S. M. Haque, H. G. O. Sandberg, H. Friedrich, V. Ermolov, Graphene-flakes printed wideband elliptical dipole antenna for low-cost wireless communications applications. *IEEE Antennas Wireless Propag. Lett.* **16**, 1883–1886 (2017).

Citation: A. Sarycheva, A. Polemi, Y. Liu, K. Dandekar, B. Anasori, Y. Gogotsi, 2D titanium carbide (MXene) for wireless communication. *Sci. Adv.* **4**, eaau0920 (2018).

Science Advances

2D titanium carbide (MXene) for wireless communication

Asia Sarycheva, Alessia Polemi, Yuqiao Liu, Kapil Dandekar, Babak Anasori and Yury Gogotsi

ARTICLE TOOLS	http://advances.sciencemag.org/content/4/9/eaau0920
SUPPLEMENTARY MATERIALS	http://advances.sciencemag.org/content/suppl/2018/09/17/4.9.eaau0920.DC1
REFERENCES	This article cites 39 articles, 1 of which you can access for free http://advances.sciencemag.org/content/4/9/eaau0920#BIBL
PERMISSIONS	http://www.sciencemag.org/help/reprints-and-permissions

Use of this article is subject to the Terms of Service